Draft version January 18, 2001
Preprint typeset using LaTeX style emulateapj v. 14/09/00

X-RAY LINE PROFILES FROM PARAMETERIZED EMISSION WITHIN AN ACCELERATING STELLAR WIND

Stanley P. Owocki
Bartol Research Institute, University of Delaware, Newark, DE 19716
E-mail: owocki@bartol.udel.edu

David H. Cohen
Department of Physics and Astronomy, Swarthmore College, Swarthmore, PA 19081
E-mail: dcohen1@swarthmore.edu

Draft version January 18, 2001

ABSTRACT

Motivated by recent detections by the *XMM* and *Chandra* satellites of X-ray line emission from hot, luminous stars, we present synthetic line profiles for X-rays emitted within parameterized models of a hot-star wind. The X-ray line emission is taken to occur at a sharply defined co-moving-frame resonance wavelength, which is Doppler-shifted by a stellar wind outflow parameterized by a 'beta' velocity law, $v(r) = v_\infty(1 - R_*/r)^\beta$. Above some initial onset radius R_o for X-ray emission, the radial variation of the emission filling factor is assumed to decline as a power-law in radius, $f(r) \sim r^{-q}$. The computed emission profiles also account for continuum absorption within the wind, with the overall strength characterized by a cumulative optical depth τ_*. In terms of a wavelength shift from line-center scaled in units of the wind terminal speed v_∞, we present normalized X-ray line profiles for various combinations of the parameters β, τ_*, q and R_o, and including also the effect of instrumental broadening as characterized by a Gaussian with a parameterized width σ. We discuss the implications for interpreting observed hot-star X-ray spectra, with emphasis on signatures for discriminating between "coronal" and "wind-shock" scenarios. In particular, we note that in profiles observed so far the substantial amount of emission longward of line center will be difficult to reconcile with the expected attenuation by the wind and stellar core in either a wind-shock or coronal model.

Subject headings: radiative transfer — shock waves — stars: early-type — stars:mass-loss — X-rays: stars — X-rays: line-profiles

1. INTRODUCTION

Over the past two decades, orbiting X-ray observatories from *Einstein* to *ASCA* have shown that both hot and cool stars are moderately strong sources of soft X-rays at energies from 0.1 to 2 keV. For cooler, late-type stars, the scaling of X-ray luminosity with, e.g., stellar rotation, suggests a solar-type origin, with surface magnetic loops confining hot, X-ray-emitting material within nearly static circumstellar coronae. For hotter, early-type stars, the X-ray luminosity has no discernible dependence on rotation, but instead scales nearly linearly with bolometric luminosity, $L_{\rm x} \approx 10^{-7} L_{\rm Bol}$ (Long & White 1980; Pallavicini et al. 1981; Chlebowski, Harnden, & Sciortino 1989), suggesting a different emission mechanism, perhaps related to the high-density, radiatively driven stellar wind observed from such stars.

Nonetheless, an ongoing question has remained whether such hot-star X-ray emission originates from coronal-like processes occuring in nearly static regions near the stellar surface (Cassinelli & Olson 1979; Waldron 1984; Cohen, Cassinelli, & MacFarlane 1997), or rather in the highly supersonic wind outflow, perhaps from shocks arising from intrinsic instabilities in the radiative driving mechanism (Lucy & White 1980; Lucy 1982; Owocki, Castor, & Rybicki 1988; Feldmeier et al. 1997; Feldmeier, Puls, & Pauldrach 1997; Owocki & Cohen 1999). Based on the observed strong winds in hot stars (e.g., Snow & Morton 1976), a key discriminant has been the apparent general lack of soft X-ray absorption, which, along with optical and UV spectral constraints, implies limits to the extent, temperature, and fractional contribution of the total X-ray output from a base corona (Cassinelli, Olson, & Stalio 1978; Nordsieck, Cassinelli, & Anderson 1981; Cassinelli & Swank 1983; Baade & Lucy 1987; MacFarlane et al. 1993; Cohen et al. 1996). This limited inferred absorption is thus generally seen as evidence for emission arising from lower-density regions at large radii, in general agreement with a wind-shock model.

In the context of extreme ultraviolet spectroscopy, MacFarlane et al. (1991) presented models of emission line profiles, from both a coronal source and from an expanding shell, affected by transfer through a stellar wind. These authors demonstrated that emission line profiles are a key discriminant of the source location. However, due to the small throughput and modest resolution of the *Extreme Ultraviolet Explorer* (*EUVE*) spectrometers, combined with the extreme opacity of the interstellar medium in this bandpass, emission lines from only one hot star (ϵ CMa) were observed with *EUVE.* The only high signal-to-noise line seen in this EUV spectrum was the He II Lyα line, which was observed to be broadened by several hundred km s^{-1}, lending credence to models that postulate a wind-origin for the hot plasma in OB stars (Cassinelli et al. 1995).

It is only recently, however, that orbiting X-ray observatories like *XMM* and *Chandra* have been able to provide the first detections of spectrally resolved X-ray emission lines from hot, luminous stars (Kahn et al. 2001; Schulz et al. 2001; Waldron & Cassinelli 2001). Through the broadened profiles of these resolved X-ray emission lines, these data provide a new, key diagnostic for inferring whether the X-ray emission originates from a nearly static corona, or from an expanding stellar wind outflow. A key goal of the present paper is to provide a firm basis for interpreting such X-ray emission line spectra.

Specifically, we describe below the method (§2) and results (§3) for computations of synthetic line profiles arising from parameterized forms of X-ray emission in an expanding stellar wind. In comparison to recent work by Ignace (2001), who derived analytic forms for X-ray emission profiles for the case of constant expansion velocity, our analysis takes into account a variation of velocity $v(r)$ in radius r, as parameterized by the so-called 'beta-law' form $v(r) = v_\infty (1 - R_*/r)^\beta$, where R_* is the stellar radius and v_∞ is the wind terminal speed. As in Ignace (2001), the overall level of attenuation is characterized by an integral optical depth τ_*, and the X-ray emission filling factor is assumed to decline outward as a power law in radius, $f(r) \sim r^{-q}$. However, we also allow for this emission to begin at a specified onsent radius R_o that can be set at or above the surface radius R_*. We first present scaled emission profiles for various combinations of the four parameters β, τ_*, q, and R_o (§3.1). For selected cases intended to represent roughly the competing models of a "base coronal" emission vs. instability-generated "wind-shock" emission, we next compute synthetic profiles that are broadened by the estimated instrumental resolution for emission lines observed by *XMM* and *Chandra* (§3.2). We then present a collection of profiles for lines which, based on line-center energy, are taken to have systematically different characteristic values for formation radius R_o, continuum optical depth τ_*, and instrumental broadening σ (§3.3). Finally, we discuss (§4) how various features of the synthetic profiles are influenced by properties of the emitting material, and outline prospects for future work in interpreting hot-star X-ray spectra.

2. COMPUTING X-RAY LINE EMISSION FROM A SPHERICAL STELLAR WIND

Extended monitoring observations by X-ray missions like *ROSAT* (Berghöfer & Schmitt 1994) have shown that for most early-type stars the X-ray emission is remarkably constant, with little or no evidence of rotational modulation, and with overall variations at or below the 1% level. This suggests that the hot, X-ray emitting material must be well-distributed within the circumstellar volume, whether in a narrow, near-surface corona, or as numerous ($n > (1/0.01)^2 = 10^4$), small elements of shock-heated gas embedded in the much cooler, UV-line-driven, ambient stellar wind. Here we model any such complex structure in terms of a spherically symmetric, smooth distribution of X-ray line emission, with emissivity $\eta_\lambda(r,\mu)$ at an observer's wavelength λ along direction cosine μ from a radius r. The resulting X-ray luminosity spectrum L_λ is given by integrals of the emission over direction and radius, attenuated by continuum absorption within the medium,

$$L_\lambda = 8\pi^2 \int_{-1}^{1} d\mu \int_{R_*}^{\infty} dr\, r^2 \eta_\lambda(\mu,r) e^{-\tau[\mu,r]}. \qquad (1)$$

2.1. *Optical Depth Integration*

The absorption optical depth $\tau[\mu,r]$ can be most easily evaluated by converting to ray coordinates $z \equiv \mu r$ and $p \equiv \sqrt{1-\mu^2}$, and then integrating over distance z for each ray with impact parameter p,

$$t[p,z] = \int_z^\infty \kappa\rho[r']\, dz', \qquad (2)$$

where $\rho[r']$ is the mass density at radius $r' \equiv \sqrt{p^2 + z'^2}$. We assume here that the X-ray absorption cross-section-per-unit-mass, κ, is a fixed constant that is independent of wavelength λ within the line and radius r within the wind. For emission at a given r along direction cosine μ, the optical depth attenuation in eqn. (1) can then be obtained through the simple substitution,

$$\tau[\mu,r] = t\left[\sqrt{1-\mu^2}\, r,\, \mu r\right]. \qquad (3)$$

For simplicity, we consider here a steady-state wind with velocity given by the 'beta-law' form $w(r) \equiv v(r)/v_\infty = (1 - R_*/r)^\beta$. Taking account also of the occultation by the stellar core of radius R_*, we then write

$$\begin{aligned} t[p,z] &= \infty \qquad\qquad ; \quad p \le R_* \ \ \& \ \ z \le \sqrt{{R_*}^2 - p^2} \\ &= \tau_* \int_z^\infty \frac{R_* dz'}{r'^2 (1 - R_*/r')^\beta} \quad ; \ \text{otherwise.} \end{aligned} \qquad (4)$$

Here we have used the mass loss rate, $\dot{M} \equiv 4\pi\rho v r^2$, to define a characteristic wind optical depth, $\tau_* \equiv \kappa\dot{M}/4\pi v_\infty R_*$. Note that in a wind with $\beta = 0$ and thus a constant velocity $v = v_\infty$, the radial ($p = 0$) optical depth at radius r would be given simply by $t[0,r] = \tau_* R_*/r$. Thus in such a contant-velocity wind, τ_* would be the radial optical depth at the surface radius R_*, while $R_1 = \tau_* R_*$ would be the radius of unit radial optical depth.

For general integer values of β, e.g. $\beta = 0$, 1, 2, or 3, it is still possible to obtain closed-form analytic expressions for the optical depth integral (4), though the expressions can be quite lengthy to write down explicitly (see also Ignace (2001)). In the present work, these analytic forms are derived and evaluated using the mathematical analysis software, *Mathematica*. For non-integer β, the optical depth integral (4) must generally be done by numerical quadrature.

2.2. *Line-Emission Integration*

Let us next consider the line emissivity, which we take here to be of the form

$$\eta_\lambda(r,\mu) = C\rho^2(r) f(r)\, \delta\left[\lambda - \lambda_o(1 - \mu v(r)/c)\right], \qquad (5)$$

where C is an emission normalization constant, λ_o is the rest wavelength for the line-emission, and $f(r)$ represents a volume filling-factor for X-ray emission. Note that the radial dependence of this filling factor may reflect variations in the temperature distribution of the plasma, as well as variations in the total emission measure. The form (5) ignores all broadening (e.g., natural, Stark, thermal, turbulent), and simply assumes the emission is an arbitrarily sharp function centered on the local, Doppler-shifted, comoving-frame wavelength $\lambda_o(1 - \mu v(r)/c)$. For convenience, let us define a scaled wavelength measured from line center in units of the wind terminal speed v_∞, i.e.

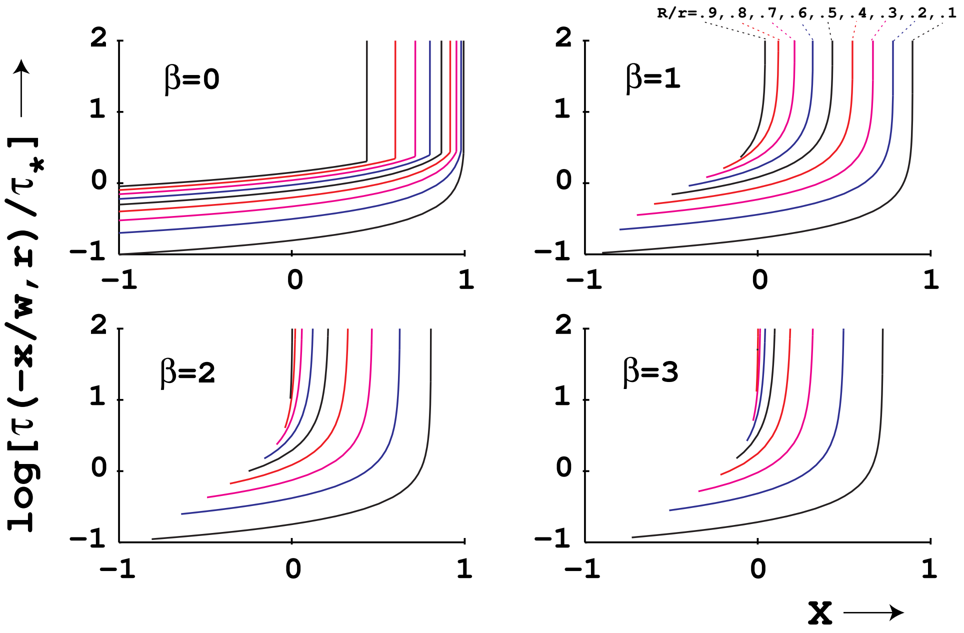

FIG. 1.— Log of the scaled optical depth $\tau[-x/w(r),r]/\tau_*$ vs. the scaled wavelength x, at selected radii r in models with $\beta = 0$, 1, 2, and 3. These contours effectively show the degree of wind attenuation as a function of wavelength for a source at a given radius.

$x \equiv (\lambda/\lambda_o - 1)c/v_\infty$. In terms of this scaled wavelength, the integrals (1) for the luminosity spectrum then become

$$L_x = 8\pi^2 C \int_{-1}^{1} d\mu \int_{R_*}^{\infty} dr\, r^2\, f(r)\rho^2(r) e^{-\tau[\mu,r]}\, \delta(x+\mu w(r))\,, \tag{6}$$

where we have used the convention $L_x dx = L_\lambda d\lambda$. Integrating the Dirac δ-function over direction cosine μ, we then find that the wavelength-dependent X-ray luminosity can be evaluated from the single radial integral,

$$L_x = \frac{C\dot{M}^2}{2v_\infty^2} \int_{R_*}^{\infty} dr\, H\left[w(r) - |x|\right]\, \frac{f(r)}{r^2 w^3(r)}\, e^{-\tau[-x/w(r),r]}\,, \tag{7}$$

where H is the Heaviside (a.k.a. unit-step) function, with $H(s) = 1$ if $s \geq 0$, and zero otherwise.

Ignace (2001) has recently derived completely analytic results for the case of a power-law emission factor $f(r) \sim r^{-q}$ and constant outflow velocity, $\beta = 0$ (implying $w(r) = 1$). As noted above, for the somewhat more general case of nonzero, but *integer* values of β, the optical depth integral (4) can still be done analytically; but in general the radial integral (7) must be evaluated by numerical quadrature. For this numerical integration, it is convenient (following Ignace (2001)) to define an inverse radius coordinate $u \equiv R_*/r$. In the case of an emission factor of the power-law form $f(r) = f_* u^q$ for radii $r \equiv R_*/u > R_o \equiv R_*/u_o$, and zero otherwise, the integral to be evaluated then becomes

$$L_x = \frac{C f_* \dot{M}^2}{2v_\infty^2 R_*} \int_0^{u_x} du \frac{u^q}{(1-u)^{3\beta}}\, e^{-\tau\left[-x/(1-u)^\beta, R_*/u\right]}\,, \tag{8}$$

where

$$u_x \equiv \min\left[u_o, 1 - |x|^{1/\beta}\right]\,. \tag{9}$$

Figure 1 plots the optical depth $\tau[-x/w(r),r]$ versus scaled wavelength x at selected radii r in models with various β. For each radius, there is a critical, positive wavelength x where the optical depth increases steeply, representing the strong attenuation of the red-wing emission by the dense inner wind and stellar core. Such core occultation makes the integrand in eqn. (8) effectively zero for all u where $(1-u)^\beta\sqrt{1-u^2} < x$. For blue-wing wavelengths $x < 0$, the termination of the curves indicates the maximum blue-shift allowed by the velocity at the relevant radius.

3. RESULTS FOR NORMALIZED X-RAY LINE PROFILES

To focus now on the general *form* of X-ray emission line profiles, let us define a normalized emission profile,

$$l_x \equiv \frac{L_x}{\max_x[L_x]}. \tag{10}$$

which simply sets the profile maximum to have value of unity. This effectively removes the dependence on the several free parameters (e.g. f_*, $\dot{M}$, v_∞, etc.) that affect the overall emission normalization. The form of the resulting X-ray line-profile l_x versus scaled wavelength x thus depends on four free parameters, viz. β, τ_*, q, and R_o/R_*. The effects of wind attenuation and other model parameters on the overall X-ray emission level have been addressed in a broad-band context by Owocki & Cohen (1999), but in focussing here on line profile shapes, we defer to future work any analysis of the overall emission line strength.

3.1. *Synthetic Emission Line Profiles for Various Model Parameters*

Figure 2 presents synthetic emission profiles for various combinations of these parameters, all plotted vs. the scaled wavelength x over the range $-1 < x < 1$. For comparison, Figure 3 shows the flat-topped profiles for corresponding cases with optically thin emission, $\tau_* = 0.01$. Some notable general properties and trends are as follows:

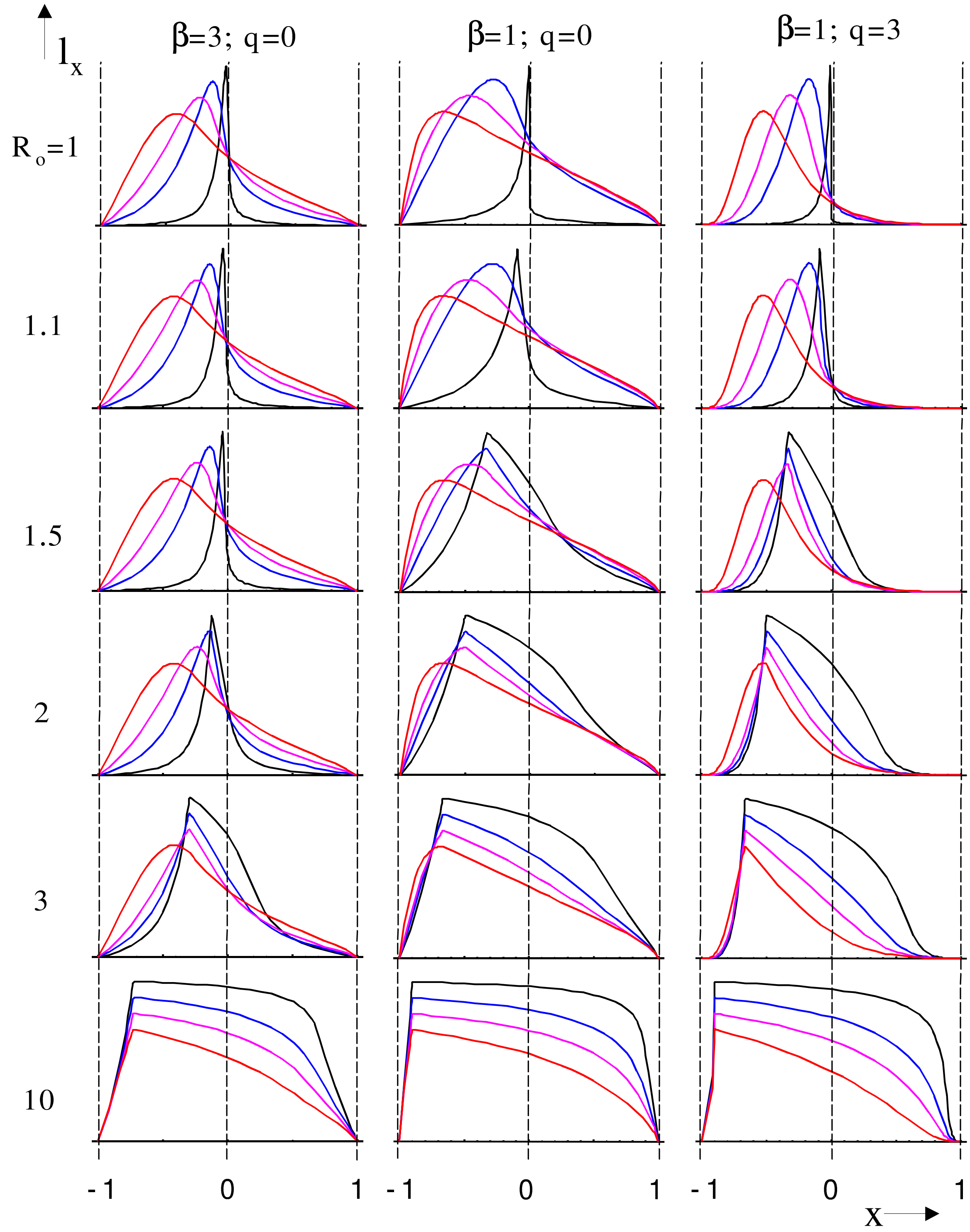

FIG. 2.— Scaled emission profile l_x vs. the scaled wavelength x, plotted for various parameter combinations. In each box, profiles for optical depths $\tau_* = 1$, 3, 5, and 10 are overplotted, with the various curves distinguished by having their peak values scaled respectively by factors of 1, 0.9, 0.8, and 0.7. The six rows represent, from the top to bottom, cases with initial emission radii of $R_o/R_* = 1$, 1.1, 1.5, 2, 3, and 10. The central of the three columns represents a 'standard' case with $\beta = 1$ and $q = 0$, while the columns to each side illustrate cases which differ from this standard by setting $\beta = 3$ (left) or $q = 3$ (right).

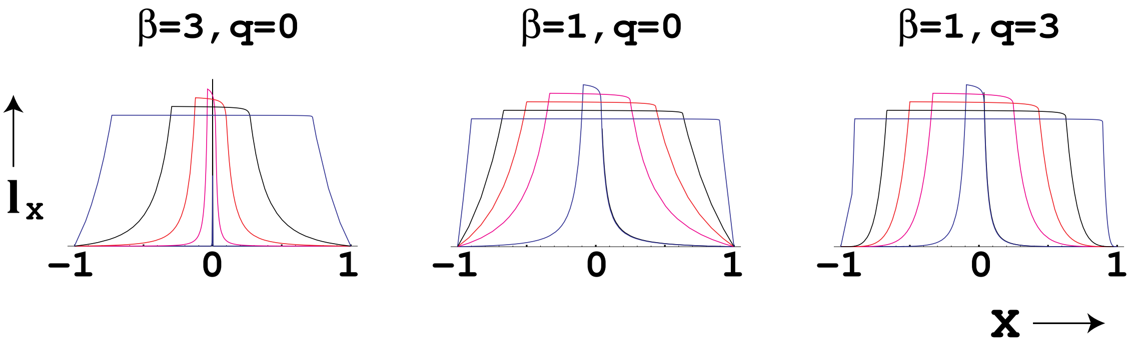

FIG. 3.— Flat-topped emission profiles for the optically thin case $\tau_* = 0.01$. The left, center, and right box correspond to the same wind parameters as in Figure 2, but the five overplots in each box now represent cases with initial emission radii at $R_o/R_* = 1.1$, 1.5, 2, 3, and 10, with the various curves now distinguished by having their peak values scaled respectively by factors of 1, 0.95, 0.9, 0.85, and 0.8.

- The profiles seem most sensitive to τ_* and R_o, with β and q having a comparatively modest influence.
- The emission peaks are always blueward of line center (i.e., at $x < 0$), with increasing blueshift for increasing τ_* and/or increasing R_o.
- The overall line-width likewise increases with increasing τ_* and/or R_o. The narrowest lines occur when both τ_* and R_o are near unity. Large τ_* with low R_o tend to give blue-shifted "peaked" forms, while large R_o tend to be blue-tilted "flat-top" forms.
- The blue-to-red slope near line center is always negative. For low τ_* it varies from very steep for low R_o to nearly flat for large R_o. For large τ_* it has a more intermediate steepness for all R_o.

3.2. *Broadened Profiles for Coronal vs. Wind-Shock Scenarios*

For the simple parameterized models used, the profiles presented above represent the expected intrinsic line emission. But line-profiles observed by *XMM* and *Chandra* can be significantly broadened by the limited spectral resolution of their detectors. To facilitate more direct comparison with such observed profiles, let us next convolve our model emission profiles with a Gaussian kernel function characterized by a broadening parameter σ, defined here in units of the wind terminal speed v_∞.

To keep the parameter range tractable, we identify specific parameter subsets to represent general conditions in the two distinct scenarios that have often been invoked in modelling hot-star X-ray emission, namely the "coronal" (e.g., Waldron 1984) vs. "wind-shock" scenarios (e.g., Feldmeier, Puls, & Pauldrach 1997; Owocki & Cohen 1999). The coronal scenario envisions X-ray emission as coming mostly from a relatively narrow, nearly static layer near the stellar surface; we represent this here with the parameter values $q = 5$, $\beta = 3$, and $R_o = R_*$. The wind-shock scenario generally envisions X-ray production arising from instability-generated shocks that form in the acceleration region $r = 1 - 3R_*$ of the star's line-driven wind, with eventual slow decay of the shocks in the outer wind; we respresent this here with the parameter values $R_o = 1.5R_*$, $\beta = 1$, and $q = 0.5$. For both scenarios we again consider the effect of various optical depth parameters, τ_*.

Figure 4 compares results for the coronal (left) vs. wind-shock (right) scenario. Here some notable general properties and trends include:

- At the best resolution ($\sigma = 0.1$), the coronal models are, as expected, notably narrower than the wind models.
- The wind-shock models are generally more blue-shifted than the coronal models.
- At the coarsest resolution, ($\sigma = 0.5$), all profiles have similar width, but still generally differ in overall blue-shift.
- For the optically thin case, the emission is nearly symmetric about line center. For other cases,

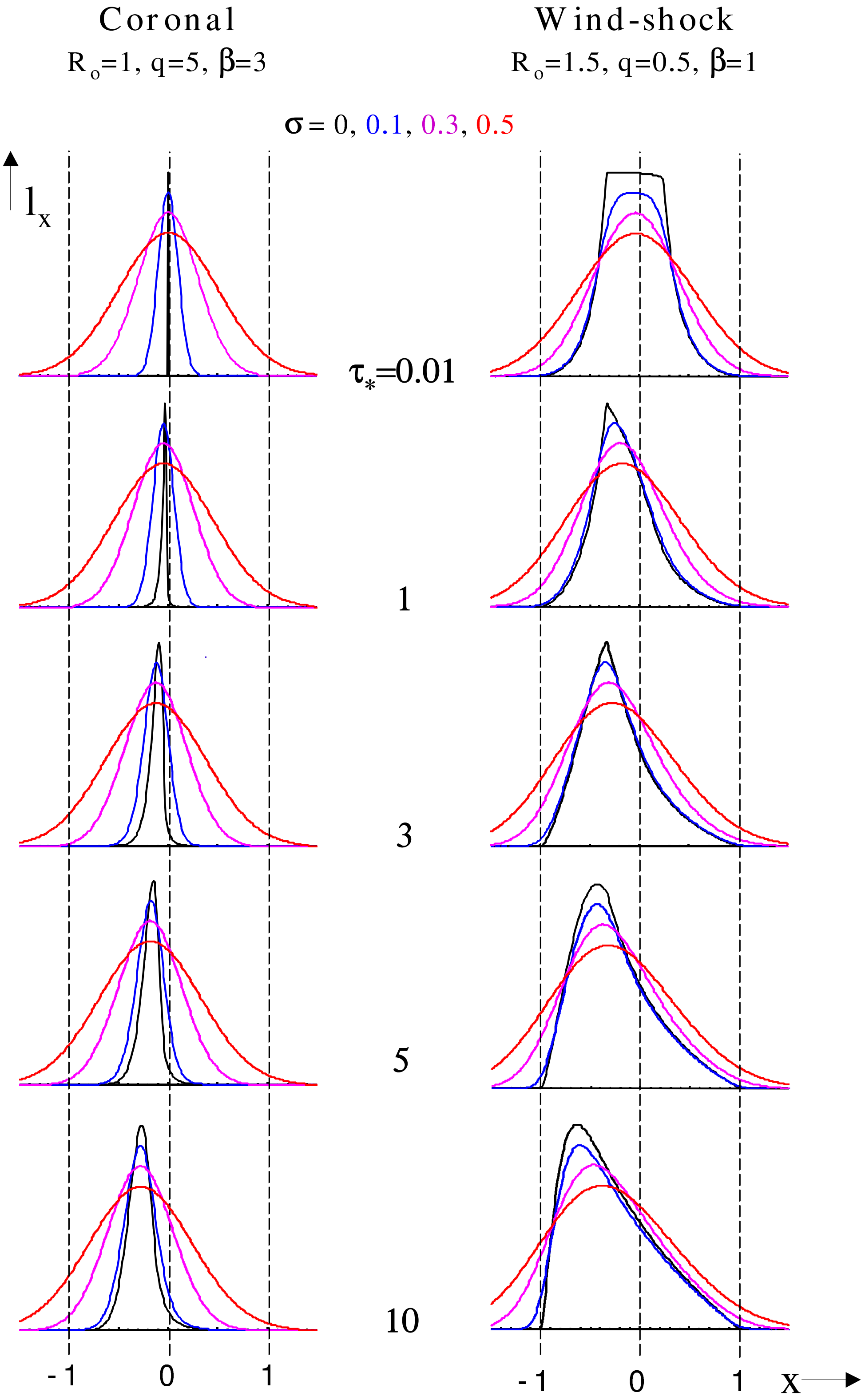

FIG. 4.— As in Figure 2, scaled emission profile l_x vs. the scaled wavelength x, but now comparing results for a coronal (left) vs. wind-shock (right) scenario. The four overplots now represent profiles with broadening parameters set to $\sigma = 0$, 0.1, 0.3 and 0.5, again with the overall emission scaled respectively by factor of 1, 0.9, 0.8, and 0.7. The five rows now represent (from the top) cases with optical depth parameters set respectively to $\tau_* = 0.01$, 1, 3, 5, and 10.

the emission peaks become more blue-shifted with increasing optical depth τ_*. The coronal model with larger τ_* may not be relevant, however, since wind absorption would greatly reduce the overall strength of any observable emission.

Clearly, at the high resolutions available with *XMM* and *Chandra* (which range down to $\sigma \approx 0.1$ depending on the line energy and the wind terminal velocity), it should be possible to place strong constraints on the site of X-ray emission and the degree of wind attenuation.

3.3. *Profiles Reflecting Energy Dependence of Optical Depth, Resolution, and Formation Radius*

To illustrate further some general issues in applying synthetic profiles toward the interpretation of observed X-ray spectra, let us next consider how the various parameters like optical depth τ_*, instrumental broadening σ, and initial radius R_o can depend on the energy of the various detectable line transitions.

First, since continuum opacity tends to decline with energy, roughly as $\kappa \sim E_x^{-2}$, we can expect that the highest energy lines should have the lowest total optical depth parameter τ_*. Second, for both *XMM* and *Chandra* the spectral broadening tends to increase with energy, scaling roughly as $\sigma \sim E$. Finally, the highest energy emission lines should form at the lowest radii, where the peak emission temperatures can be expected to occur. For the He-like and H-like iso-electronic sequences that dominate the spectrum, lines from a given element are generally in the same portion of the spectrum, with the line energy correlated with the atomic number, and therefore with the temperature of peak emissivity; but in a shock-heating model, the highest plasma temperatures can be expected to occur in the wind acceleration region, and then decline outward as the material cools by radiative losses and adiabatic expansion. Overall, we thus expect that the initial emission radius, R_o, should be lowest for highest energy lines.

Taken together, these trends imply that high-energy lines should have narrower *intrinsic* widths (smaller R_o and smaller τ_*), but suffer greater *intrumental* broadening. Conversely, the lower energy lines would be intrinsically broader (larger R_o and larger τ_*) but be intrumentally better resolved. These overall trends may account for the relatively uniform line widths seen in the initial *XMM* spectrum of ζ Pup (Kahn et al. 2001) and the *Chandra* spectrum of ζ Ori (Waldron & Cassinelli 2001). Moreover the overall concept of a variable formation radius for each line, corresponding to optical depth unity in the wind, has also been inferred based on helium-like line-ratio diagnostics (Kahn et al. 2001; Waldron & Cassinelli 2001; Cassinelli, Miller, & MacFarlane 2000).

Figure 5 illustrates explicitly these kinds of trends of line properties with energy. The central panel plots intrinsic profiles for lines formed at various initial radii R_o (setting $\tau_* = 0.5R_o/R_*$), while the side panels show corresponding profiles with characteristic broadening expected for *Chandra* (left) and *XMM* (right). As noted, the instrumental resolution compensates for the intrinsic broadening, making the observed widths quite similar. However, there are still some differences in the line shapes, with the lines formed at a greater R_o being more skewed and blue-shifted.

4. DISCUSSION

The parameterized emission models here provide a good basis for interpreting X-ray line-profile observations made possible by the new generation of orbiting X-ray telescopes. While detailed, quantitative analyses must await the general availability of specific datasets, it is already clear from the few hot-star X-ray spectra published thus far that there are some noteworthy challenges for modeling the associated X-ray emission. For example, temperature-sensitive line-ratio diagnostics imply quite high temperatures (the extreme case is θ^1 Ori C with $T > 5 \times 10^7$ K; Schultz et al. 2000), while helium-like forbidden-to-intercombination line ratios imply either very high densities (up to $n_e \approx 10^{14}$ cm^{-3}) or very close proximity to the photosphere ($r < 1.1\ R_*$) (Miller, Cassinelli, & MacFarlane 2000).

Most notably in the present context, there are also some quite puzzling characteristics in the observed line profiles. For example, in the *XMM* spectrum of ζ Pup (Kahn et al. 2001), the lines all exhibit a similar, significant broadening, but with half-widths $\sim 1000 - 1500$ km s^{-1} that are still somewhat lower than the inferred wind terminal speed $v_\infty \gtrsim 2000$ km s^{-1}. Moreover, the typical profiles have a rounded, Gaussian form that is quite distinct from, e.g., the flat-topped profiles expected for optically thin emission from a nearly constant velocity expansion. Finally, the profiles show only modest asymmetry, with the peak intensity only slightly blue-shifted, by $\sim 0 - 400$ km s^{-1} relative to line-center, and the red-wing only slightly flatter and more extended than the blue-wing.

It is difficult to reconcile these profile characteristics (viz. substantial broadening, but little asymmetry and blueshift) with a model that includes attenuation by the wind and stellar core, both of which should preferentially attenuate X-rays from the back-side hemisphere; in a wind or a corona with some outflow, this should preferentially reduce the red-side emission. In fact, from detailed modeling constrained by *ROSAT* observations, Hillier et al. (1993) have argued that that the wind of ζ Pup should be optically thick to 1 keV X-rays at 10 R_*, with the radius of optical depth unity being even greater for softer X-rays (20 R_* at 0.6 keV; and still 2 R_* at 2 keV).

Even for a base corona with some overall outflow velocity and *no* overlying wind attenuation, occultation by the stellar core should still produce line profiles that are skewed toward the blue. A coronal model with little or no net outflow could explain the observed profile symmetry, but matching the observed line-widths would then require the coronal material to have extremely large "turbulent" motions. For example, line widths in the XMM observations of ζ Pup by Kahn et al. (2001) require velocity dispersions of up to 1500 km s^{-1}, and some of the lines observed by *Chandra* in θ^1 Ori C are even broader than this (yet apparently still nearly symmetric).

Our synthesized line profiles from *wind* models are capable of producing relatively broad, yet symmetric and unshifted profiles, but only in the nearly complete absence of wind attenuation. Any wind shock model with significant wind attenuation is expected to be strongly blueshifted

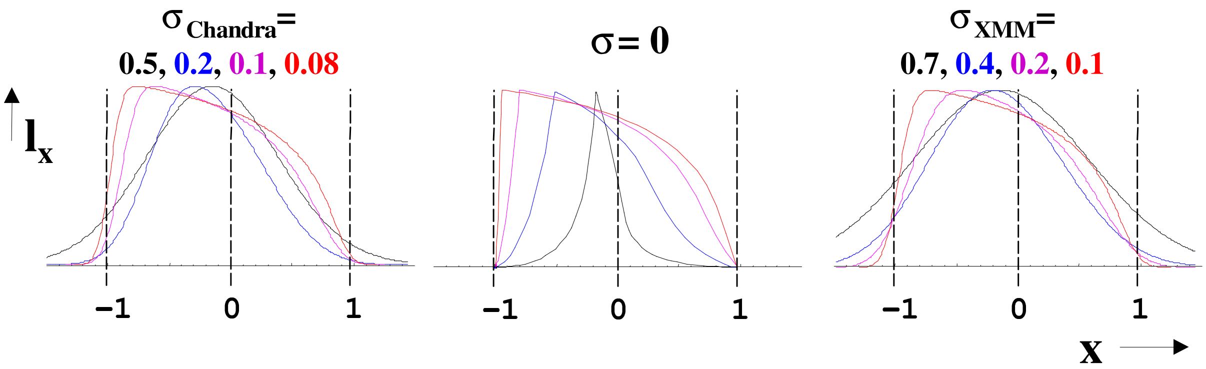

FIG. 5.— Scaled emission profile l_x vs. the scaled frequency x for fixed trends in line properties correlated with line energy. The basic emission model has $\beta = 1$ and $q = 0.5$. The four overplotted profiles correspond to lines formed at $R_o = 1.2$, 2, 5, and 20 R_*, and with optical depths $\tau_* = 0.5\ R_o/R_*$. The central panel shows the unbroadened emission profiles, with greater blue-shift of the peak corresponding to larger R_o. On each side are profiles broadened according to fixed sequences, namely $\sigma = 0.5$, 0.2, 0.1, 0.08 (left) and $\sigma = 0.7$, 0.4, 0.2, 0.1 (right), chosen roughly to correspond the range of line resolutions in hot-star observations by *Chandra* (left) and *XMM* (right). These sets of profiles are intended to illustrate expected general trends, but do not correspond directly to any specific star or data set.

and quite asymmetric (see Figure 4). Of all the line profiles discussed in the first group of *XMM* and *Chandra* papers, perhaps the N VII Lyα profile at 24.8 Å in the *XMM* spectrum of ζ Pup provides the strongest indication of a wind origin for the observed X-rays (Kahn et al. 2001). The authors find that this line has a blueshift of 400 km s^{-1} and a half-width at half-maximum of 1600 km s^{-1}. Although they fit the line with a Gaussian, they comment on its apparent asymmetry, which is qualitatively in accord with what we calculate here for models with a large X-ray onset radius, R_o.

In summary, systematic fitting of the line-profiles will be necessary to place more quantitative constraints on the spatial distribution of hot plasma and the degree of wind attenuation in the observed O stars; but some initial qualitative inferences are already possible. The implied minimal wind attenuation combined with some significant bulk motion are puzzling, both in the context of coronal X-ray emission and in the context of the strong radiation-driven winds that are known to exist on these stars from UV, optical, IR, and radio observations. One possible solution to the wind attenuation problem might be found in clumping. A "porous" wind might allow many of the X-rays to stream through unattenuated, yet also lead to significant UV absorption if the interclump wind medium still has sufficient column density to produce optically thick UV lines. (The UV line transition probabilities are significantly larger than the bound-free X-ray cross sections.) An alternative is that the mass-loss rates of O stars may have been overestimated. It is not likely, however, that the winds are dense and smooth but transparent to X-rays, as that would require levels of ionization in the wind that would not allow for efficient radiation-driving. And, if the winds are indeed optically thin, then to discriminate between coronal and wind models will require a careful analysis of the shifts and asymmetries observed in the X-ray line profiles.

Finally, although we developed our analysis with hot stars in mind, it can be applied to any X-ray source in which lines are emitted within a spherically symmetric expanding medium that may also have substantial continuum opacity. This could include nova winds, planetary nebulae, active galactic nuclei, and X-ray binaries.

We thank R. Ignace for providing a preprint of his paper on analytic X-ray profiles and also for his detailed comments on this manuscript, K. Gayley and A. Ud-Doula for helpful comments on our analysis, and J. Cassinelli and J. MacFarlane for many useful insights regarding the X-ray spectra of O stars. This research was supported in part by NASA grant NAG5-3530 to the Bartol Research Institute at the University of Delaware.

REFERENCES

Baade, D., & Lucy, L. 1987, A&A, 178, 213

Berghöfer, T. W., & Schmitt, J. H. M. M. 1994, Ap&SS, 221, 309

Cassinelli, J. P., Cohen, D. H., Macfarlane, J. J., Drew, J. E., Lynas-Gray, A. E., Hoare, M. G., Vallerga, J. V., Welsh, B. Y., Vedder, P. W., Hubeny, I., & Lanz, T. 1995, ApJ, 438, 932

Cassinelli, J. P., Miller, N. A., & MacFarlane, J. J. 2000, *High Energy Astrophysics Division Meeting*, 32, 45.04

Cassinelli, J. P., & Olson, G. L. 1979, ApJ, 229, 304

Cassinelli, J. P., Olson, G. L., & Stalio, R. 1978, ApJ, 220

Cassinelli, J. P., & Swank, J. H. 1983, ApJ, 271, 681

Chlebowski, T., Harnden, F. R., Jr., & Sciortino, S. 1989, ApJ, 341, 427

Cohen, D. H., Cooper, R. G., MacFarlane, J. J., Owocki, S. P., Cassinelli, J. P., & Wang, P. 1996, ApJ, 460, 506

Cohen, D. H., Cassinelli, J. P., & MacFarlane, J. J. 1997, ApJ, 487, 867

Feldmeier, A., Kudritzki, R.-P., Palsa, R., Pauldrach, A. W. A., & Puls, J. 1997, A&A, 320, 899

Feldmeier, A., Puls, J., & Pauldrach, A. W. A. 1997, A&A, 322, 878

Hillier, D. J., Kudritzki, R. P., Pauldrach, A. W., Baade, D., Cassinelli, J. P., Puls, J., & Schmitt, J. H. M. M. 1993, A&A, 276, 117

Ignace, R. 2001, ApJ, submitted

Kahn, S. M., Leutenegger, M. A., Cotam, J., Rauw, G., Vreux, J.-M., den Boggende, A. J. F., Mewe, R., & Güdel, M. 2001, A&A, in press

Long, K. S., & White, R. L. 1980, ApJ, 239, L65

Lucy, L. 1982, ApJ, 255, 286

Lucy, L. B., & White, R. L. 1980, ApJ, 241, 300

Macfarlane, J. J., Cassinelli, J. P., Welsh, B. Y., Vedder, P. W., Vallerga, J. V., & Waldron, W. L. 1991, ApJ, 380, 564

MacFarlane, J. J., Waldron, W. L., Corcoran, M. F., Wolff, M. J., Wang, P., & Cassinelli, J. P. 1993, ApJ, 419, 813

Miller, N. A., Cassinelli, J. P., & MacFarlane, J. J. 2000, *High Energy Astrophysics Division Meeting*, 32, 42.06

Nordsieck, K. H., Cassinelli, J. P., & Anderson, C. M. 1981, ApJ, 248, 678

Owocki, S. P., Castor, J. I., & Rybicki, G. B. 1988, ApJ, 335, 914

Owocki, S. P., & Cohen, D. H. 1999, ApJ, 520, 833

Pallavicini, R., Golub, L., Rosner, R., Vaiana, G. S., Ayres, T., & Linsky, J. L. 1981, ApJ, 248, 279

Schulz, N. S., Canizares, C. R., Huenemoerder, D., & Lee, J. C. 2001, ApJ, in press

Snow, T. P., Jr., & Morton, D. C. 1976, ApJS, 32, 429

Waldron, W. L. 1984, ApJ, 282, 256

Waldron, W. L., & Cassinelli, J. P. 2001, ApJ, in press